Enhanced 20th century heat transfer to the Arctic simulated in the context of climate variations over the last millennium

J.H. Jungclaus, K. Lohmann, and D. Zanchettin

{Max Planck Institut für Meteorologie, Hamburg, Germany}

Correspondence to: J. H. Jungclaus (johann.jungclaus@mpimet.mpg.de)

Abstract

Oceanic heat transport variations, carried by the northward flowing Atlantic Water, strongly influence Arctic sea-ice distribution, ocean-atmosphere exchanges, and pan-Arctic temperatures. Paleoceanographic reconstructions from marine sediments near Fram Strait have documented a dramatic increase in Atlantic Water temperatures over the 20th century, unprecedented in the last millennium. Here we present results from Earth system model simulations that reproduce and explain the reconstructed exceptional Atlantic Water warming in Fram Strait in the 20th century in the context of natural variability during the last millennium. The associated increase in ocean heat transfer to the Arctic can be traced back to changes in the ocean circulation in the sub-polar North Atlantic. An interplay between a weakening overturning circulation and a strengthening sub-polar gyre as a consequence of 20th century global warming is identified as driving mechanism for the pronounced warming along the Atlantic Water path toward the Arctic. Simulations covering the late Holocene provide a reference frame that allows us to conclude that the changes during the last century are unprecedented in the last 1150 years and that they cannot be explained by internal variability or natural forcing alone.

1 Introduction

The Arctic is one of the regions where climate change has been diagnosed most drastically in terms of warming and sea-ice decline over the last decades. Direct temperature measurements are, however, scarce and only available for the last century. Reliable observations of sea-ice evolution are even more limited, covering only the satellite era. On decadal timescales, internal variations can substantially contribute to Arctic climate variability (Bengtsson et al., 2004; Beitsch et al., 2014) and the relative role of external drivers is still under debate (Booth et al., 2012; Zhang et al., 2013). High-resolution reconstructions of paleoclimatic variables over the late Holocene provide a reference frame and put recent changes in context with long-term natural variations. Ongoing efforts, such as the Past Global Changes 2K network (PAGES2K, Ahmed et al. 2013) initiative, provide regional syntheses of reconstructions that can be compared with model simulations. While most of the PAGES2K reconstructions rely on terrestrial proxies, high-quality marine paleodata become increasingly available at annual to decadal resolution. Novel proxies have been developed to reconstruct, for example, dynamical quantities such as near-bottom flow strength in the Nordic Seas overflow regions (e.g., Mjell et al. 2014). Of particular value are reconstructions from key locations, such as major conduits of the large-scale ocean circulation. Spielhagen et al. (2011) and Dylmer et al. (2013) have published records from marine sediments off Svalbard that reflect temperature changes in the Atlantic Water (AW) in Fram Strait over the last 2000-3000 years. The time series show centennial-scale modulations of the AW temperatures and, as a pronounced common feature, a dramatic, unprecedented warming over the 20th century. The authors speculate that the observed warming reflect considerable changes in the lateral heat transfer to the Arctic that might have contributed to the rapid warming and sea-ice decrease during the 20th century.

Earth system model simulations over the last millennium provide a tool to test such hypotheses, and to investigate the relative role of internal variability on the one hand, and natural and anthropogenic forcing on the other hand. Provided that the model adequately simulates regional-scale features, simulations also allow for attributing locally observed variations to changes in large-scale dynamics.

In general, the model results have to be confronted with observations and reconstructions to assess in how far they reproduce the real climate evolution, both in direct comparison (e.g., Fernandez-Donado et al. 2012) and in a statistical sense (Bothe et al., 2013). In this paper, we use the results of Max Planck Institute Earth System Model (MPI-ESM) simulations for the last millennium and the industrial period to address the following research questions:

1. Can the simulations reproduce important features of reconstructed climate indicators in high northern latitudes during the last millennium and in the 20th century, both on a continental and local scale?
2. How exceptional is the observed 20th century AW warming in Fram Strait in the context of the climate evolution during the last millennium, and what implications does it have for the heat transfer to the Arctic?
3. What are the mechanisms behind the observed and reconstructed changes?

Regarding the latter, we concentrate in this paper on the 20th century changes in high northern latitudes and the North Atlantic and devote a subsequent study to pre-industrial variations and their relation to external forcing. The paper is organized as follows. In section 2, we describe the MPI-ESM model set-up and the boundary conditions applied for the simulations covering the last millennium. Results for integrated high-northern latitude changes and the evolution of the Atlantic Water transfer from the North Atlantic to the Arctic are given in section 3. In section 4, we formulate a dynamical interpretation of the results and discuss implications for 20th century climate change in the North Atlantic realm in section 5. Main conclusions are given in section 6.

2. The Model system and the experimental design of the last millennium simulations

The model employed in this study is the Max Planck Institute Earth System Model (MPI-ESM). MPI-ESM and its various configurations contributing to the Coupled Model Intercomparison Project, phase 5 (CMIP5), have been documented in a special issue of the Journal for Advances in Modeling Earth Systems (JAMES). The configuration for Paleo applications (MPI-ESM-P) used here is identical

79 with the MPI-ESM-LR configuration described in the JAMES publications by Giorgetta et al. (2013)
80 and Jungclaus et al. (2013) with two exceptions: First, the dynamic vegetation module is switched off
81 in order to allow for the implementation of land-cover change maps (Pongratz et al. 2008) as in the
82 earlier, lower-resolution model version described by Jungclaus et al. (2010). Second, the orbital
83 forcing is prescribed by a table providing annual values for eccentricity, obliquity and perihelion,
84 whereas the LR version uses a calendar-based orbit. The atmosphere model ECHAM6 (Stevens et al.
85 2013) is run at a horizontal resolution of spectral truncation T63 (1.875°) and 47 vertical levels,
86 resolving the stratosphere up to 0.01 hPa. The ocean/sea-ice model MPIOM (Marsland et al. 2003;
87 Jungclaus et al. 2013) features a conformal mapping grid with nominal 1.5° resolution and 40 vertical
88 levels (GR1.5L40). It is noteworthy for our study that the GR1.5L40 grid possesses one grid pole over
89 Antarctica and one grid pole over Greenland, which leads to considerably higher resolution in the
90 regions of interest for this study, i.e. the northern North Atlantic (Jungclaus et al. 2008). In Fram
91 Strait, for example, the grid size in cross-channel direction is about 30-40 km. The simulations over
92 the last millennium (past1000) follow the protocol of the Paleo Modeling Intercomparison Project,
93 phase 3 (PMIP3). As part of this protocol, Schmidt et al. (2011) summarize different choices for
94 external forcing and boundary conditions and provide tables for well mixed-greenhouse gases (CO_2,
95 CH_4, N_2O), and orbital parameters. In contrast to the millennium simulations described in Jungclaus
96 et al. (2010), which featured an interactive carbon-cycle and prognostic CO_2, we use prescribed CO_2
97 in the past1000 runs analyzed here. We employed the Crowley and Unterman (2013) reconstruction
98 for volcanic aerosol optical depth and effective radius and the Pongratz et al. (2008) reconstruction
99 of global land-cover and agricultural areas. For solar radiation we have followed the approach
100 described in Schmidt et al. (2011) combining the Vieira et al. (2011) total solar irradiance (TSI)
101 reconstruction over the Holocene with the Wang et al. (2005) data set that provides the
102 recommended solar forcing for the CMIP5 20^{th} century (1850 – 2005) simulations. An artificial 11-yr
103 cycle of varying amplitude is imposed over the pre-industrial period (see Schmidt et al., 2011 for
104 details). Linear interpolation was used to calculate monthly TSI averages from the reconstructed

105 annual TSI values for the period 850-1849 scaled to Total Irradiance Monitor (TIM) data, except for
106 the flux at 180.5 nm. Spectral Solar Irradiance (SSI) for the 14 short-wave spectral bands of the
107 ECHAM6's radiation scheme was calculated so that the sum of SSI yields TSI. Energy in the part of the
108 spectrum below the shortest wavelength of the radiation scheme (200nm) and above the longest
109 (12195.1 nm) was added to the first and last band, respectively. Monthly average ozone
110 concentrations for the period 850-1849 are calculated using the 1850-1860 monthly climatology of
111 ozone concentrations from the AC&C/SPARC Ozone Database as a basis and representing the ozone
112 dependency on solar irradiance through regression coefficients between historical ozone
113 concentrations and the annual 180.5 nm solar flux. An 1155 year-long pre-industrial control
114 integration (PiCtrl) under fixed 1850 boundary conditions serves as a reference simulation for forced
115 experiments. To conduct the past1000 simulations we first ran a 400 year-long adaptation simulation
116 starting from the end of piCtrl to adjust to 850 boundary conditions and thereafter started the three
117 realizations past1000-r1, past1000-r2, and past1000-r3. The past1000-r1 and past1000-r2
118 experiments were initialized with the same ocean state, but differ in the standard deviation of the
119 assumed lognormal distribution of the volcanic aerosol size (1.2 µm in r1, 1.8 µm in r2 and r3). The
120 simulations past1000-r2 and past1000-r3 used the same parameter setting but were started from
121 different initial conditions. Furthermore, ozone concentration data used in past1000-r1 are affected
122 by use of a 1-month-shifted annual cycle in the AC&C/SPARC ozone climatology, an issue solved in
123 past1000-r2 and –r3. While the three simulations are therefore not an ensemble of three runs
124 carried out with an identical model and forcing/boundary conditions, we consider the effect of the
125 different setting small enough to regard the runs as three realizations of possible last millennium
126 climate evolution under parameter and forcing uncertainties. The PMIP3 protocol defines the
127 past1000 integration period as 850-1849. To relate the recent climate evolution to the late-Holocene
128 variability we continued the respective past1000 simulations over the historical period (1850 – 2005).
129 The applied boundary conditions follow the CMIP5 protocol, except for land-cover-changes, where
130 we continue the simulations with the Pongratz et al. (2008) data set. In the following, we refer to the

131 combined past1000 and historical simulations covering the period 850-2005 as pr1, pr2, and pr3,
132 respectively. Since the emphasis of our present study is on the 20th century changes, we also include
133 in some analyses in section 4 and 5 one additional MPI-ESM-P "historical" (hr1) simulation (1850-
134 2005), which was initialized from the PiCtrl experiment.
135

136 3. Last millennium evolution of high northern latitude climate

137 3.1 Pan-Arctic temperature and sea-ice extent

138 We start the analyses with quantities that reflect the general climate evolution in high northern
139 latitudes. Reconstructing regional-scale temperature and other climate variables such as sea-ice
140 extent in sparsely-sampled areas is still challenging. Only recently pan-Arctic reconstructions for
141 temperature have been published (Kaufman et al., 2009; Shi et al. 2012), mostly based on terrestrial
142 proxies (tree-rings) and ice cores. The PAGES2K consortium reviewed reconstruction data and
143 methods and constructed seven continental-scale temperature records, including the Arctic (Ahmed
144 et al. 2013). The reconstructed temperature records (black lines in Figure 1 a) have in common that
145 they show a gradual cooling during the last millennium, possibly reflecting the overall evolution from
146 a warmer Medieval Warm Period (MWP) to an anomalously cold Little Ice Age (LIA). Note that the
147 PAGES2K record reflects annual mean temperatures whereas the other two represent the summer
148 season. All reconstructions (and the instrumental data that they are matched to) show a strongly
149 reversed trend during the 20th century. The Shi et al. (2012) and Kaufman et al. (2009) summer
150 temperature reconstructions disagree on the magnitude of the pre-industrial cooling. This reflects
151 differences in the proxies chosen, their geographical distribution, and the statistical methods used to
152 match the proxies to historical observations. We are not in a position to judge which of the two time
153 series reflects more appropriate the real climate evolution; we therefore regard the discrepancy as a
154 measure of uncertainty in reconstructed climate. The simulated summer temperatures are
155 compatible with the reconstructions and match closely the Kaufman et al. (2009) data. Individual
156 simulations (colored lines in Figure 1 a) show relatively strong fluctuations and ensemble realizations

157 differ often quite strongly (about 0.5°C) for a given period. In contrast to global and hemispheric
158 averages (not shown here, but see Figure 5 in Jungclaus et al. 2010), individual volcanic eruptions
159 (like the very strong 1258 or 1453 tropical eruption) or clusters of volcanic events are not clearly
160 discernible, with the exception of the 1809 and 1815 (Tambora) eruptions, where all simulations
161 show a similar cold excursion, in accordance with the Kaufman and Past2K reconstructions. The
162 resilience to volcanic forcing reflects the relatively small signal-to-noise ratio of Arctic summer
163 temperatures, due to both strong internal variability of the Arctic regional climate (e.g. Beitsch et al.,
164 2014) and seasonal character of local response mechanisms, which are most prominent in boreal
165 winter (e.g., Zanchettin et al., 2012). Zanchettin et al. (2013) have also highlighted the role of
166 background conditions (e.g. during the closely following 1809 and 1815 eruptions) for the actual
167 response patterns, in particular at high latitudes. The Arctic warming throughout the 20th century is
168 also well reflected in the model simulations and the pronounced variations such as the warm phase
169 in the first half of the last century are well within the ensemble range of the historical experiments.
170 The summer sea-ice reconstruction by Kinnard et al. (2011) comes with a relatively large range of
171 uncertainty (dashed black lines in Fig. 1b) but the main characteristic is that of a mirror-image of the
172 pan-Arctic surface temperature evolution: A gradual increase in sea-ice extent during the pre-
173 industrial millennium is replaced by a drastic decline in the 20th century (Figure 1 b). The decline of
174 sea-ice extent sets in, however, more abruptly in the mid-20th century in contrast to the relatively
175 gradual warming. The past1000 simulations reproduce a similar long-term trend over the pre-
176 industrial millennium and the 20th century simulations terminate at an extent that is equally low as
177 the observations. In the simulations, the sea-ice decline begins, however, earlier featuring a temporal
178 evolution more similar to the pan-Arctic temperature (Figure 1a). In fact, all four historical
179 simulations show ice extent anomalies below the reconstruction's mean estimate between 1870 and
180 1950. The sea-ice reconstruction exhibits a pronounced relative minimum in the late 16th century,
181 which none of the three past1000 simulations reproduces. Notwithstanding questions regarding
182 uncertainties in the reconstructions, it is difficult to relate the event to known volcanic or solar

forcing variations (e.g. the minimum around 1700 appears at the time of the Maunder minimum in solar variations). The anomalies in the 15th to 17th century exceed the 2-sigma range of control experiment variability significantly. We have detected events of similar magnitude in unforced control simulations, but they appear only rarely (once in a 1000-yr simulation). It is therefore possible that the model underestimates internal variability of the sea-ice extent.

3.2 Fram Strait Atlantic Water temperatures

The reconstructions of AW temperatures stem from a marine core at site MSM5/5-712 at 78°54.94'N, 6°46.04'E (see Spielhagen et al. (2011) and Werner et al. (2011) for details). The authors provide two temperature records, one based on a modern analogue technique (SIMMAX), and one based on the Magnesium-Calcium (Mg/Ca) ratio of *Neogloboquadrina pachyderma*. Habitat and plankton bloom estimates indicate that both proxies reflect mid-summer conditions in the upper part of the AW layer. During pre-industrial times, the Mg/Ca-derived record exhibits much stronger variability, which might reflect inaccuracies in recording the cold-water range (Spielhagen et al., 2011). Both reconstructions, however, fluctuate around very similar pre-industrial mean values (3.4° and 3.6°C) and indicate a warming of roughly 2°C during the 20th century (Figure 2). A similar temperature increase is also found in continued measurements from Svalbard fjords from 1912 to 2005 (Pavlov et al., 2013) and agrees with previous estimates of 20th century evolution of AW properties in the northern North Atlantic (Polyakov et al., 2004). Another late-Holocene sedimentary record from Malangen Fjord in northern Norway (Hald et al. 2011) reflects local variations in the influx of AW and shows a similar temperature evolution over the last 1200 years including an unprecedented warming in modern times.

We compare the Spielhagen et al. (2011) reconstructions with simulated fluctuations of temperatures in the AW core at 50m depth in Fram Strait at about 78°N (Figure 2). The relatively low temporal resolution and the strong fluctuations in the Mg/Ca record prohibit a very detailed comparison in the pre-industrial millennium. The simulations and the SIMMAX data agree in a change

209 from slightly warmer-than-average temperatures in the first centuries and colder conditions in the
210 16th to 18th centuries, reflecting the general change from MWP to LIA conditions. Interestingly, all
211 time-series show a cold spell in the early 19th century, likely recording the 1809 and 1815 eruptions.
212 During the 20th century, simulations and the SIMMAX record agree in a 2°C warming. The simulations
213 also exhibit considerable decadal to multidecadal variations that are not covered or sub-sampled by
214 the reconstructions' resolution. The ensemble spread and the relatively large variability range
215 obtained from the unforced control run (Figure 2), points to a large fraction of internal variability.
216 Clearly, the warming in the industrial period exceeds the 2σ-range of the undisturbed simulation.
217 Spielhagen et al. (2011) speculate that the diagnosed warming infers a considerable increase in heat
218 transfer to the Arctic. In the model simulations, we can quantify the heat flux changes and display in
219 Figure 3a the combined total ocean heat transport (TOHTR) through Fram Strait and through the
220 Barents Sea Opening (BSO), which both show the unprecedented increase in the 20th century. Firstly,
221 we confirm that the AW temperature record reflects indeed changes in heat transfer through the
222 most important conduits towards the Arctic. The correlation coefficients between AW temperatures
223 and TOHTR (smoothed by a 31-yr running mean) exceed 0.9 at zero time-lag in all three past1000
224 simulations. Simulated TOHTR anomalies are shown with respect to (w.r.t.) the pre-industrial (850-
225 1849) mean of about 80 TW (1 TW = 10^{12} Watt). The simulated transports are compatible with
226 observations indicating a heat transport of 30-40 TW in Fram Strait (Schauer et al., 2008) and 30-76
227 TW in BSO (Årthun et al., 2012). Observations of heat transports are, however, only available for the
228 most recent decades and may be influenced by decadal-scale variability as well. During the pre-
229 industrial period, there are TOHTR fluctuations of the order of 10-20 TW and the ensemble indicates
230 somewhat higher-than-normal TOHTR in the early part of the simulation and less TOHTR in the 16th
231 and 17th century. Large volcanic eruptions (1258, 1453, and 1815) leave an imprint on the heat
232 transports leading to reduction of heat transfer to the Arctic (Zanchettin et al., 2012). The most
233 pronounced feature of our smoothed time series from the simulations is, however, a consistent

234 increase of up to 30 TW during the 20th century, reflecting a 40% increase over the pre-industrial
235 mean.
236 The modulation of the AW temperature could either be driven by local changes in the wind system
237 (Bengtsson et al., 2004) or be part of variations in the warm water path associated with the North
238 Atlantic Current or the Atlantic Meridional Overturning Circulation (AMOC), as has been suggested,
239 for example by Polyakov et al. (2004). However, recently Lozier (2010) and Lozier et al. (2010) have
240 demonstrated that overturning and gyre circulation in the North Atlantic are strongly linked and that
241 the image of a continuous conveyor belt associated with the AMOC may be misleading. Building on
242 earlier results analyzing Arctic warming events in an unperturbed control integration (Beitsch et al.,
243 2014) we therefore decompose the (TOHTR) in the Atlantic basin into its overturning and gyre
244 components (MOHTR, and GOHTR, respectively). The first reflects the zonal average heat transport,
245 the second the deviations of the zonal average (e.g. Eden and Jung, 2001; Drijfhout and Hazeleger,
246 2006). First, we calculate the correlations between the TOHTR at the entrance to the Arctic (Figure
247 3a) and the components of the basin-scale OHTRs for all latitudes. High correlations are found in
248 particular in the sub-polar North Atlantic between GOHTR and heat transfer to the Arctic (not
249 shown). At the entrance to the Nordic Seas at 60°-65°N (Figure 3b) we can see that most of the
250 modulation in the heat transfer to the Artic during the millennium can be traced back to downstream
251 fluctuations in GOHTR. The gyre heat transport features multi-centennial changes from stronger-
252 than-normal conditions in the early centuries of the simulation to weaker conditions during the Little
253 Ice Age. The 20th century stands out again with its unprecedented increase in the TOHTR. Most of the
254 increase at 60-65°N is carried by an increase in the gyre component, but, interestingly, also the
255 overturning component shows a clear positive trend over the 20th century and apparently
256 contributes to high-latitude warming despite the fact that AMOC is decreasing at 30°N over the 20th
257 century.
258
259 **4. Origin of the 20th century heat transfer increase**

In the following, we focus on the changes in the 20th century and elucidate the relation between heat transfer changes in Fram Strait and the sub-polar North Atlantic. We consider simulated linear 100yr trends (1905-2005) and compare them with the expected range of internal variability as expressed in the 5-95 percentile range of the respective variables taken from the 1000 yr-long PiCtrl simulation.

The changes in the heat transport components over the 20th century reflect trends in the large-scale ocean circulation. Figure 4 shows the centennial trends for the AMOC streamfunction (Figure 4a) as function of latitude and for the barotropic horizontal streamfunction (Figure 4b) together with their long-term means. The AMOC increases at higher-latitudes, but the most prominent feature is a broad-scale weakening in subtropical and subpolar latitudes at depth below 1000m. As has been described in previous studies (e.g. Latif et al., 2006), this weakening is associated with reduced deep-water formation, most prominently in the Labrador Sea (see below). On the other hand, the circulation cell reaching into the Nordic Seas strengthens as more overturning occurs at higher latitudes. The barotropic streamfunction trends are characterized mainly by a pronounced strengthening (the negative sign refers to more cyclonic circulation) in the central and eastern part of the subpolar basin. In the central Labrador Sea, the gyre circulation weakens, which is, again, compatible with reduced deep water formation in the main convection region. There is also indication of a weakening of the gyre circulation in the Nordic Seas.

The change in TOHTR in the Atlantic basin reflects the trends in its components: in particular in sub-polar latitudes, a weaker overturning component is mostly compensated by a stronger gyre component (Figure 5a), but the resulting TOHTR does not exceed the range of internal variability. North of 55°N changes in both components are much smaller, but are constructively adding up to positive TOHTR trends. The trends are robust in the four simulations, and the 20th century TOHTR trends exceed the 5-95% range deduced from the PiCtrl run in three of the four simulations. In subtropical latitudes, overturning transports are also smaller, but not compensated by the gyre transports. Thus the TOHTR here are considerably weaker and exceed the 5-95% range of trends in the control simulation. Meridional divergence or convergence of TOHTR then causes regional cooling

286 or warming, if not compensated by surface heat fluxes. Therefore, positive slopes of the TOHTR
287 curves in Fig. 5a indicate cooling while negative slope indicate warming, as indicated by the red and
288 light-blue horizontal lines at the bottom of Figure 5aa. Regions, where divergence of advective lateral
289 heat transport cools the ocean (Figure 5a) are associated with positive atmosphere-ocean heat flux
290 trends, indicating that the colder ocean is cooling the atmosphere. Hence the atmosphere is damping
291 the ocean-induced changes rather than enforcing them. Trends in the upper-ocean temperatures are
292 negative roughly between 45° and 60°N and, since they are only partly compensated by freshening
293 (not shown), there are considerable changes in the density structure as is shown for the pr2
294 experiment in Figure 6 (results are similar for all simulations). Increased density in the center and
295 more pronounced doming of the subpolar isopycnals is typical for a strengthening gyre. The
296 increasing horizontal density gradients, on the other hand, indicate higher baroclinic pressure
297 gradients and further accelerate the gyre (Greatbatch et al., 1991; Levermann and Born, 2007).
298 A possible reason for the acceleration of the gyre circulation could be changes in the wind system.
299 Modulations of large-scale atmospheric pressure patterns like the North Atlantic Oscillation or the
300 East Atlantic Pattern leave their specific imprint on the wind-driven ocean circulation (Häkkinen and
301 Rhines, 2009) and may be important also on centennial time scales (e.g., Sedláček and Mysak, 2009).
302 In particular, the gyre would respond to changes in the wind-stress curl caused, for example, by a
303 poleward shift of the westerlies due to global warming (e.g. Saenko et al., 2005). The centennial
304 trends in the zonal wind stress component are indeed relatively coherent in the past1000
305 experiments and resemble those obtained by Saenko et al. (2005) in idealized CO_2-doubling
306 experiments: stronger positive wind stress north of 40°N and slightly negative values in the sub-
307 tropical region (Figure 7a). While consistent in three of the four experiments considered here, the
308 changes are well within the 5-95%tile range obtained from the unperturbed control experiment.
309 Moreover, trends in wind-stress curl (Figure 7b) indicate coherent changes only in the Southern
310 Hemisphere (not shown), which is, again, consistent with the findings by Saenko et al. (2005), who
311 applied somewhat stronger CO_2 forcing.

To further elucidate the origin of the circulation changes we identify first the reason for the weakening of the AMOC in the subtropical and subpolar North Atlantic. A key ingredient modulating the AMOC here is the strength of deep water formation in the Labrador Sea (Latif et al., 2006; Lohmann et al., 2014). To quantify the latter we calculate the thickness of the Labrador Sea Water (LSW) in the region (for details, see Lohmann et al., 2014). Normalizing the anomalies, we see a clear co-variability with the AMOC at 30N and 1500m depth when AMOC lags by roughly 8-10 years. Next, we establish a link between LSW thickness and surface properties by correlating LSW thickness with the surface density field (not shown), which reveals the central Labrador Sea as convection hot-spot. The evolution of surface density, temperature and salinity in the so-identified region reveals, as expected, that enhanced LSW formation comes together with positive density anomalies at the surface that reduce the static stability and induce convection. Also shown in Figure 8a are the corresponding temperature and salinity time series. Following the evolution through the last three centuries indicate pronounced multi-decadal variability and pronounced differences between the industrial period and the centuries before. The multidecadal variability is characterized by co-varying temperature and salinity, where apparently, density is determined by the salinity changes (e.g., fresher and lighter conditions lead to less dense surface waters, which is not compensated by colder temperatures). The variations in the regional fresh-water budget is mainly caused by modulations of the sea-ice and fresh water supply from higher latitudes (Jungclaus et al., 2005) and from redistribution of zonal salinity transport by the Irminger Current. During the 20th century, however, this relation breaks down as somewhat fresher conditions (also caused by increasing sea-ice and fresh-water export through Denmark Strait, not shown) go along with a general warming, partly caused by direct radiative forcing, partly be redistribution of heat by an enhanced Irminger Current. As a result, AMOC weakens at latitudes downstream from the LSW formation region. The temporal evolution of the vertical density structure in the Labrador Sea indicates then generally less dense

conditions in the upper 2000m. Interestingly, the deepest layers are characterized by relatively colder temperatures and higher densities that are caused by the enhanced overturning in the Nordic Seas and associated changes in the strength and density of the Denmark Strait overflow. Changes in the vertical density structure are important for the east-west density gradient driving the AMOC (Lozier et al., 2010), but also affect the baroclinic structure of the gyre directly (Drijfhout and Hazeleger, 2006).

5. Discussion

Our analysis has demonstrated that the increasing heat transports to higher latitudes are mainly caused by changes in the gyre and overturning circulation in the subpolar North Atlantic. These changes are caused by a reduction in deep water formation in the Labrador Sea, which leads to reduced overturning circulation in subtropical and subpolar latitudes. In addition, changes in the vertical structure of water masses at the western boundary can modify the baroclinic gyre circulation (Drijfhout and Hazeleger, 2006). The associated changes in MOHTR and GOHTR lead to enhanced TOHTR towards higher latitudes and heat transport divergence (cooling) in the subpolar region.5 The colder and denser SPG then spins up baroclinically, which further increases the GOHTR (dashed lines in Figure 5a), which, in turn, extracts even more heat from the SPG center and further increases the horizontal density gradient. Thus a positive feedback mechanism is initiated. The mechanism can be compared to the one described by Levermann and Born (2007) and Born et al. (2013a). These authors describe a positive feedback, where an (somehow) accelerated gyre leads to increasing east-west temperature and salt transports along its northern rim. Increasing salinity then leads to denser surface waters in the Labrador Sea and to enhanced convective activity, which further spins up the gyre. In our simulations, we see also a redistribution of salinity during the 20th century change in gyre circulation resulting in higher salinities in the western part of the basin. However, in contrast to the mechanism described by Levermann and Born (2007), the positive temperature anomalies dominate the near-surface density evolution in the industrial period and Labrador Sea convection rather

decreases. Levermann and Born (2007) demonstrated that a bistability regime exists, where the transition between the two regimes can be triggered by small fluctuations in surface freshwater flux. Born et al. (2013a) extended the study and found multiple circulation modes in PiCtrl experiments in six out of 19 models (among them MPI-ESM-LR). Even though we find some differences to their mechanism, it is possible that the relatively strong response of the SPG is an expression of such a transition, here triggered by changes in the AMOC. Possibly also the wind-stress changes (Figure 7) play a role in initiating the change in the gyre circulation by modified Ekman and/or Sverdrup transports. Furthermore, gyre circulation changes can also directly be driven by changes in the baroclinic structure at the western boundary as has been shown in the global warming simulations by Drijfhout and Hazeleger (2006). At the western boundary near the exit of the Labrador Sea (Figure 8b), the density changes are consistent with a weakening of Labrador Sea Water production and an increase in overflow-derived density, similar to what has been found by Drijfhout and Hazeleger (2006). It is difficult, however, to exactly detect which component is more important in initially triggering the mechanism. For this, additional sensitivity experiments (e.g., partial-coupling experiments) would be necessary, which is beyond the scope of this study. In any case, an important ingredient is the weakening of the AMOC in subtropical and subpolar latitudes, caused by a decrease in Labrador Sea Water formation as a response to global warming, while the deep water production in the Nordic Seas is even slightly enhanced. The exact mechanisms of how gyre and overturning circulations interact are also difficult to disentangle. In the historical simulations, changes in AMOC and SPG circulation appear to happen more or less instantaneous, whereas analyses of the unperturbed control simulation suggest that AMOC variations are leading by a few years.

Many CMIP5 models feature a reduction of the AMOC strength already in the 20th century (Drijfhout et al., 2012). A characteristic feature of these simulations is the “warming hole” above the sub-polar North Atlantic that can also be identified in observations (e.g. in the HadSST data set; Rayner et al., 2006). A cool surface temperature spot within the intensified SPG is also characteristic for our 20th century simulations (Figure 6) and related to the mechanism described above. Drijfhout et al. (2012)

390 decompose the temperature pattern in a radiatively forced and an AMOC fingerprint and conclude
391 that the cold sub-polar North Atlantic is indeed related to an AMOC decline. Kim and An (2012) come
392 to a similar conclusion analyzing CO_2-doubling experiments from the Coupled Model Intercomparison
393 Project Phase 3 data base.
394 Another indication that the mechanism described here is at work in reality comes from
395 paleoceanographic reconstructions for the late Holocene. Miettinen et al. (2012) compare the
396 temporal evolution of ocean temperatures at two locations, the Voering Plateu in the Norwegian Sea
397 and the SPG region south of the Reykjanes Ridge. They find that low-frequency fluctuations occur
398 out-of-phase: the Voering Plateau record features, for example, a cold anomaly during the Little Ice
399 Age (LIA), whereas the SPG is warmer than normal during this period. Such a behavior is compatible
400 with the findings described here: A weaker SPG in the LIA (Figure 3) would feature a less dense and
401 warmer center (opposite to what is seen for the strong-gyre anomaly in Figure 6) and would
402 transport less heat to the Nordic Seas. Such out-of-phase anomalies of the barotropic stream
403 function in the SPG region and the Nordic Seas can also be seen in Figure 4b. A detailed investigation
404 of the variations and processes during the pre-industrial millennium and their relation to natural
405 forcing will be subject of a subsequent study.
406 Obtaining a comprehensive view from long-term direct observations of temperature, salinity, or
407 transports remains challenging. There exist only a few long-term time series. Many continuous
408 records, such as those from weather ships (e.g. Østerhus and Gammelsrød, 1999) cover the last
409 decades and are characterized by multi-decadal variability. The temperature measurements over the
410 20th century near Svalbard by Pavlov et al. (2013) and one of the longest time-series available at all,
411 the Kola section in the Barents Sea (e.g., Skagseth et al., 2008) support the pronounced warming in
412 the Atlantic Water branch in the industrial period. Polyakov et al. (2004) synthesized various
413 observational data sets to conclude that the intermediate Atlantic Water layer in the Arctic shows a
414 continuous warming trend that is superposed by multi-decal variability. Combining proxy data and
415 observations, Cunningham et al. (2013) compiled a synthesis of SST changes in the north-eastern

416 North Atlantic and the Nordic Seas during the last millennium. For the 20th century (their Figure 1a),
417 they report that most of the records reflecting the Atlantic Water branch along Scotland and Norway
418 indicates a warming, while other records from the sub-polar North Atlantic indicate neutral or
419 cooling conditions. High-resolution proxies from the Iceland Basin (Hall et al., 2010) over the last 230
420 years indicate cooling of SSTs in the central subpolar gyre region, which would be consistent with our
421 findings. The available SST gridded data sets HadISST (Rayner et al., 2006) and ERSSTv3 (Smith and
422 Reynolds, 2004) as well as the Simple Ocean Data Assimilation (SODA) reanalysis (Carton and Giese,
423 2008) are all characterized by a cooling trend in the subpolar gyre region (Drijfhout et al., 2012; Kim
424 and An, 2012). Polyakov et al. (2010) have used historical data from the North Atlantic Ocean and
425 decomposed the changes between the 1920s and present into non-linear trend and multi-decadal
426 variability patterns. The large-scale nonlinear trend pattern resembles the 20th century SST trend in
427 the HadISST and is characterized by cooling over the subpolar gyre (see their figure 5) and warming in
428 the subtropical North Atlantic and on the northwestern European Shelf, again compatible with our
429 results for the 20th century simulations. On the other hand, the 20th century compilation of
430 temperature and salinity data from the subpolar gyre region by Reverdin (2010) compares less well
431 with our study: the central SPG at about 60N is characterized by slightly positive temperature and
432 negative density trends.
433 Uncertainties in early observations and reconstructions preclude a definite answer to what degree
434 the findings reported here can be verified by observations. While the dynamical mechanisms
435 proposed here to explain the enhanced heat transfer to the Arctic appear largely compatible with
436 observed features in the North Atlantic, they may depend on the particular model system. Moreover,
437 as many other CMIP5 models, MPI-ESM features large SST and circulation biases in the North
438 Atlantic. In particular, the path of the Gulf Stream/North Atlantic Current is too zonal (Jungclaus et
439 al., 2013), which has direct consequences for the shape of the gyres. This may affect the warm water
440 path from the Subtropics to the Nordic Seas. Using observations and model simulations for the
441 second half of the 20th century, Hatún et al. (2005) concluded that a weaker (and less zonally-

442 extended) SPG would allow more warm and saline water to enter the Nordic Seas. Our simulations,
443 but also other CMIP5 ESMs (Born et al., 2013a; Koenigk and Bradeau, 2014) and stand-alone ocean
444 model simulations with the same ocean model as used here, but forced by reanalysis data (Müller et
445 al., 2014) suggest that a stronger SPG carries more subtropical AW into the Nordic Seas and the
446 Arctic. This discrepancy may be related to the specific situation of the late 20th century described by
447 Hatún et al. (2005), where SPG changes were mainly related to the atmospheric forcing (Häkkinen
448 and Rhines, 2009; see also Born et al., 2013b).
449 A 30 TW increase in heat transfer to the Arctic over 100 years as suggested by our simulations for the
450 20th century is an important contribution to the Arctic heat budget (Serreze et al., 2007). Dividing by
451 the area of the Arctic, it corresponds to a substantial forcing of about 2 Wm^{-2}. Jungclaus and Koenigk
452 (2010) and Beitsch et al. (2014) have shown that multidecadal variations in TOHTR to the Arctic
453 impact the Arctic climate. For positive TOHTR anomalies, the sea-ice cover decreases most
454 pronounced in the Barents Sea and causes considerable variations in ocean-atmosphere heat fluxes.
455 Although only a small fraction of the Arctic is affected, the associated warming leads to positive pan-
456 Arctic temperature anomalies. Moreover, the heat-flux changes affect the atmospheric circulation.
457 An associated feedback mechanism is the Bjerknes Compensation (Bjerknes, 1964; Shaffrey and
458 Sutton, 2006; Jungclaus and Koenigk, 2010): on multidecadal time-scales, TOHTR and atmospheric
459 heat transports (AHTR, here derived from the components of moist and dry static energy advection
460 following Keith (1995)) are strongly coupled and may compensate each other. Thus, both TOHTR and
461 AHTR need to be considered for an assessment of the lateral heat transfer changes as part of the
462 Arctic heat budget. Comparing TOHTR and AHTR at 70°N (Figure 9) indicates considerable
463 multidecadal variability, where the respective TOHTR and AHTR tend to evolve out-of-phase.
464 However, there is no compensation of the strong positive trend in TOHTR during the last decades of
465 the simulation. Therefore we conclude that there is a net positive contribution from the lateral heat
466 fluxes to the Arctic heat budget and to the warming in recent decades. An assessment of all terms of
467 the Arctic heat budget and the feedback mechanisms leading to Arctic Amplification is, however,

beyond the scope of our paper. The magnitude of TOHTR changes appears to play a decisive role in the amplitude of pan-Arctic warming, and sea-ice evolution in climate-change simulations (Mahlstein and Knutti, 2011). These authors concluded that the TOHTR changes contribute significantly to Arctic amplification, but they also identified considerable differences in the TOHTR magnitude in the CMIP3-model suite as a cause for model uncertainty in projected Arctic warming.

6. Conclusions

The MPI-ESM last-millennium simulations consistently reproduce enhanced 20th century warming of AW at the boundary between the Nordic Seas and the Arctic compared with pre-industrial variability. The warming of AW in Fram Strait is an indicator for a prominent (~40%) increase in oceanic heat transfer to the Arctic during the 20th century. In the simulations, we are able to trace back the heat transport changes to a reorganization of the large-scale ocean circulation in the sub-polar North Atlantic. The SPG and the associated northward heat transport are intensified by the global-warming-induced weakening of the AMOC and changes in the density structure associated with modified deep water formation. The latter also lead to a slight intensification of the overturning in high northern latitudes. Together, the gyre and overturning-related heat transport changes lead to an increase in the heat transfer to the Nordic Seas and the Arctic. Changes in wind-stress curl do not appear to be significantly different from the unperturbed variability, but wind-stress changes may nonetheless play a role in triggering the mechanism. Transient simulations over the late Holocene provide a valuable reference frame to discriminate unprecedented changes such as those observed in the 20th century from natural or internal fluctuations.

Acknowledgements: This work was supported by the European Community's 7th framework program (FP7/2007-2013) under the grant agreements no. 308299 (NACLIM), and no. 243908 (Past4Future). D.Z. was supported by the German Federal Ministry for Education and Research (BMBF) Miklip project (FKZ: 01LP1158A). The MPI-ESM-P simulations were conducted at the German Climate Computing Center (DKRZ). The authors thank Chao Li and two anonymous reviewers for comments that helped improving the manuscript. The service charges for this open access publication have been covered by the Max Planck Society.

References:

Ahmed, M. and the PAGES 2k Consortium: Continental-scale temperature variability during the last two millennia, Nature Geosci., 6, 339–346, doi:10.1038/ngeo1797, 2013.

Årthun, M., Eldevik, T., Smedsrud, L.H., Skagseth, Ø., Ingvaldsen, R.B.: Quantifying the influence of Atlantic heat on Barents Sea ice variability and retreat, J. Climate, 25, 4736-4743, doi:10.1175/JCLI-D-11-00466.1, 2012.

Beitsch, A., Jungclaus, J.H., and Zanchettin, D.: Patterns of decadal-scale Arctic warming events in simulated climate. Clim. Dynam., 43, 1773-1789 doi:10.1007/s00382-013-2004-5, 2014.

Bengtsson, L., Semenov, V.A., and Johannessen, O.M.: The early twentieth-century warming in the Arctic – a possible explanation. J. Climate, 18, 4045-4057, doi:10.1175/1520-0442(2004)017<4045:TETWIT>2.0.CO;2, 2004.

Bjerknes, J.: Atlantic air-sea interaction, Adv. Geophys., 10, 1-82, 1964.

Booth, B.B.B., Dunstone, N.J., Halloran, P.R., Andrews, T., and Bellouin, N.: Aerosols implicated as a prime driver of twentieth century North Atlantic climate variability, Nature, 484, 228-232, doi:10.1038/nature10946, 2012.

Born, A., Stocker, T.F., Raible, C.C., and Levermann, A.: Is the Atlantic subpolar gyre bistable in comprehensive climate models? Clim. Dynam, 40, 2993-3007, doi:10.1007/s00382-012-1525-7, 2013a.

Born, A., Stocker, T.F., and Sandø, A.B.: Coupling of eastern and western subpolar North Atlantic: salt transport in the Irminger Current, Ocean Sci. Discuss., 10, 555-579, 2013b.

Bothe, O., Jungclaus, J.H., and Zanchettin, D.: Consistency of the multi-model CMIP5/PMIP3 ensemble, Clim. Past, 9, 2471-2487, doi:10.5194/cp-9-2471-2013201, 2013.

Carton, J.A., and Giese, B.S.: A reanalysis of ocean climate using Simple Ocean Data Assimilation (SODA). Mon. Weather Rev., 136, 2999-3017, doi: 10.1175/2007MWR1978.1, 2008.

Crowley, T.J., and Unterman, M.B.: Technical details concerning development of a 1200 yr proxy index for global volcanism, Earth Syst. Sci. Data, 5, 187-197, doi:10.5194/essd-5-187-2013, 2013.

Cunningham, L., Austin, W.E.N., Knudsen, K.L., Eiriksson, J., Scourse, J.D., Wanamaker, A.D. Jr., Butler, P.G., Cage, A.G., Richter, T. Husum, K., Hald, M., Andersson, C., Zorita, E., Linderholm, H.W., Gunnarson, B.E., Sicre, M.-A., Sejruo, H.P., Jiang, H., and Wilson, R.: Reconstructions of surface ocean conditions from the northeast Atlantic and Nordic Seas during the last millennium. The Holocene, 23, 921-935, doi:10.1177/0959683613479677, 2013.

Drijfhout, S.S., and Hazeleger, W.: Changes in MOC and gyre-induced Atlantic Ocean heat transport, Geophys Res. Lett., 33, L07707, doi:10.1029/2006GL025807, 2006.

Drijfhout, S., van Oldenborgh, G.J., and Cimatoribus, A.: Is a decline of AMOC causing the warming hole above the North Atlantic in observed and modeled warming patterns? J. Climate, 25, 8373-8379, doi:10.1175/JCLI-D-12-00490.1, 2012.

Dylmer, C.V., Giradeau, J., Eynaud, F., Husum, K., De Vernal, A.: Northward advection of Atlantic water in the eastern Nordic Seas, Clim. Past, 9, 1505-1518, doi:10.5194/cp-9-1505-2013, 2013.

Eden, C., and Jung, T.: North Atlantic interdecadal variability: oceanic response to the North Atlantic Oscillation (1865-1997), J. Climate, 14, 676-691, 2001.

Fernández-Donado, L., González-Rouco, J.F., Raible, C.C., Ammann, C.M., Barriopedro, D., García-Bustamante, E., Jungclaus, J.H., Lorenz, S.J., Luterbacher, J., Phipps, S.J., Servonnat, J., Swingedouw, D., Tett, S.F.B., Wagner, S., Yiou, P., and Zorita, E.: Large-scale temperature response to external forcing in simulations and reconstructions of the last millennium, Clim.Past, 9, 393-421, doi:10.5194/cp-9-393-2013, 2013.

Giorgetta, M. A., Jungclaus, J. H., Reick, C. H., Legutke, S., Brovkin, V., Crueger, T., Esch, M., Fieg, K., Glushak, K., Gayler, V., Haak, H., Hollweg, H.-D., Ilyina, T., Kinne, S., Kornblueh, L., Matei, D., Mauritsen, T., Mikolajewicz, U., Mueller, W. A., Notz, D., Raddatz, T., Rast, S., Redler, R., Roeckner, E., Schmidt, H., Schnur, R., Segschneider, J., Six, K., Stockhause, M., Wegner, J., Widmann, H., Wieners, K.-H., Claussen, M., Marotzke, J., and Stevens, B.: Climate and carbon cycle changes from 1850 to 2100 in MPI-ESM simulations for the Coupled Model Intercomparison Project phase 5, J. Adv. Model Earth Syst., 5, 1–26, doi:10.1002/jame.20038, 2013.

Greatbatch, R., Fanning, A., Goulding, A., and Levitus, S.: A diagnosis of interpentadal circulation changes in the North Atlantic, J. Geophys. Res., 96, 22,009-22,023, 1991.

Häkkinen, S., and Rhines, P.B.: Shifting surface currents in the northern North Atlantic, J. Geophys. Res., 114, C04005, doi:10.1029/2008JC004883, 2009.

Hald, M., Salomonsen, G.R., Husum, K., and Wilson, L.J.: A 2000 year record of Atlantic Water temperature variability from Malangen Fjord, northeastern North Atlantic, The Holocene, 21, 1049-1059, doi:10.1177/095968361140057, 2011.

Hall, I.R., Boessenkool, K.P., Barker, S., McCave, N., and Elderfield, H.: Surface and deep ocean coupling in the subpolar North Atlantic during the last 230 years. Paleoceanography, 25, PA2101, doi:10.1029/2009PA001886, 2010.

Hátún, H., Sandø, A.B., Drange, H., Hansen, B., and Valdimarsson, H.: Influence of the Atlantic subpolar gyre on the thermohaline circulation. Science, 309, 1841-1844, doi:10.1126/science.1114777, 2005.

Jungclaus, J.H., Haak, H., Mikolajewicz, U., and Latif, M.: Arctic-North Atlantic interactions and multidecadal variability of the meridional overturning circulation. J.Climate, 18, 4016-4034, 2005.

Jungclaus, J.H., Macrander, A., and Käse, R.H.: Modelling the overflow across the Greenland-Scotland Ridge, in: Arctic-subarctic ocean fluxes, edited by Dickson, R.R., Meincke, J., and Rhines, P., Springer, Dordrecht, 527-549, 2008.

Jungclaus, J.H., Lorenz, S.J., Timmreck, C., Reick, C.H., Brovkin, V., Six, K., Segschneider, J., Giorgetta, M.A., Crowley, T.J., Pongratz, J., Krivova, N.A., Vieira, L.E., Solanki, S.K., Klocke, D., Botzet, M., Esch, M., Gayler, V., Haak, H., Raddatz, T.J., Roeckner, E., Schnur, R., Widmann, H., Claussen, M., Stevens, B., and Marotzke, J.: Climate and carbon-cycle variability over the last millennium, Clim. Past, 6, 723-737, doi:10.5194/cp-6-723-2010, 2010.

Jungclaus J.H., and Koenigk, T.: Low-frequency variability of the Arctic climate: the role of oceanic and atmospheric heat transport variations. Clim. Dynam., 34, 265-279, doi:10.1007/s00382-009-0569-9, 2010.

Jungclaus, J.H., Fischer, N., Haak, H., Lohmann, K., Marotzke, J., Matei, D., Mikolajewicz, U., Notz, D., and von Storch, J.-S.: Characteristics of the ocean simulations in the Max Planck Institute Ocean Model (MPIOM) the ocean component of the MPI-Earth system model, J. Adv. Model Earth Syst., 5, 422-446, doi:10.1002/jame.20023, 2013.

Kaufman, D.S., Schneider, D.P., McKay, N.P., Ammann, C.M., Bradley, R.S., Briffa, K.R., Miller, G,H., Otto-Bliesner, B.L., Overpeck, J.T., Vinther, B.M., and Arctic Lakes 2K project members: Recent warming reverses long-term Arctic cooling. Science, 325, 1236-1239, doi:10.1126/science.1173983, 2009.

586 Keith, D.W.: Meridional energy transport: uncertainty in zonal means. Tellus, 47A, 30-44, 1995.

587 Kim, H., and S.-I. An: On the subarctic North Atlantic cooling due to global warming. Theor. Appl.
588 Climatol., 114, 1-19, doi:10.1007/s00704-012-0805-9, 2012.

589 Kinnard, C., Zdanowicz, C.M., Fisher, D.A., Isaksson, E., De Vernal, A., and Thompson, L.G.:
590 Reconstructed changes in Arctic sea ice over the last 1,450 years. Nature, 479, 509-513,
591 doi:10.1038/nature10581, 2011.

592 Koenigk, T., and Brodeau, L.: Ocean heat transport into the Arctic in the twentieth and twenty-first
593 century in EC-Earth, Clim. Dynam., 42, 3101-3120, doi:10.1007/s00382-013-1821-x ,2014.

594 Latif, M., Böning, C., Willebrand, J., Biastoch, A., Dengg, J., Keenlyside, N., Schweckendiek, U., and
595 Madec, G.: Is the Thermohaline Circulation Changing?. J. Climate, 19, 4631–4637, doi:
596 http://dx.doi.org/10.1175/JCLI3876.1, 2006.

597 Levermann, A., and Born, A.: Bistability of the Atlantic subpolar gyre in a coarse-resolution climate
598 model. Geophys. Res. Lett., 34, L24605, doi:10.1029/2007GL031732, 2007.

599 Lohmann, K., Jungclaus, J.H., Matei, D., Mignot, J., Menary, M., Langehaug, H.R., Ba, J., Gao, Y.,
600 Otterå, O.H., Park, W., and Lorenz, S.: The role of subpolar deep water formation and Nordic Seas
601 overflows in simulated multidecadal variability of the Atlantic meridional overturning circulation.
602 Ocean Sci., 10, 227-241, doi:10.5194/os-10-227-2014, 2014.

603 Lozier, M.S.: Deconstructing the Conveyor Belt, Science, 328, 1507-1511,
604 doi:10.1126/science.1189250, 2010.

605 Lozier, M.S., Roussenov, V., Reed, M.S.C., and Williams, R.G.: Opposing decadal changes for the
606 North Atlantic meridional overturning circulation. Nature Geosci., 3, 728-734,
607 doi:10.1038/NGEO947, 2010.

608 Mahlstein I., and Knutti, R.: Ocean heat transport as a cause for model uncertainty in projected Arctic
609 warming, J. Climate, 24, 1451-1460, doi:10.1175/JCLI3713.1 ,2011.

610 Marsland, S.J., Haak, H., Jungclaus, J.H., Latif, M., and Roeske, F.: The Max- Planck- Institute global
611 ocean/sea-ice model with orthogonal curvilinear coordinates, Ocean Modelling, 5, 91-127, 2003.

612 Miettinen, A., Divine, D., Koç, N., Godtliebsen, F., and Hall, I.R.: Multicentennial variability of the sea
613 surface temperature gradient across the subpolar North Atlantic over the last 2.8kyr, J. Climate,
614 25, 4205-4219, doi:10.1175/JCLI-D-11-00581.1, 2012.

615 Mjell, T.L., Ninnemann, H.F., H.F. Kleiven, and Hall, I.R.: Multidecadal changes in Iceland-Scotland
616 overflow water vigori over the last 600 years and its relation to climate. Under review: Geophys.
617 Res. Lett., 2014.

618 Müller, W.A., Matei, D., Bersch, M., Jungclaus, J.H., Haak, H., Lohmann, K., Compo, G.P.,
619 Sardeshmukh, P.D., and Marotzke, J.: A 20th century reanalysis-forced ocean model to reconstruct
620 the North Atlantic climate variations during the 1920s. Clim. Dynam., in press: doi:
621 10.1007/s000382-014-2267-5, 2014.

622 Østerhus, S., and Gammelsrød, T.: The abyss of the Nordic Seas is warming. J. Climate, 12, 3297-3304,
623 1999.

624 Pavlov, A., Tverberg, V., Ivanov, B., Nilsen, F., Falk-Petersen, S., and Granskog, M.: Warming of
625 Atlantic Water in two west Spitsbergen fjords over the last century (1912-2009). Polar Research,
626 32, 11206, doi:10.3402/polar.v32i0.11206, 2013.

627 Polyakov, I.V., Alekseev, G.V., Timokhov, L.A., Bhatt, U.S., Colony, R.L., Simmons, H.L., Walsh, D.,
628 Walsh, J.E., Zakharov, V.F.: Variability of the Intermediate Atlantic Water of the Arctic Ocean over
629 the last 100 years, J. Climate, 17, 4485-4497, 2004.

630 Polyakov, I.V., Alexeev, V.A., Bhatt, U.S., Polyakova, E.I., and Zhang, X.: North Atlantic warming:
631 patterns of long-term trend and multidecadal variability. Clim. Dynam., 34, 439-457,
632 doi:10.1007/s00382-008-0522-3, 2010.

633 Pongratz J., Reick, C.H., Raddatz, T., and Claussen, M.: A reconstruction of global agricultural areas
634 and land cover for the last millennium, Glob. Biogeochem. Cycles, 22, GB3018,
635 doi:10.1029/2007GB003153, 2008.

636 Rayner, N.A., Brohan, P., Parker, D.E., Folland, C.K., Kennedy, J.J., Vanicek, M., Ansell, T.J., and Tett,
637 S.F.B.: Improved analyses of changes and uncertainties in sea surface temperature measured in
638 situ since the mid nineteenth century: the HadSST2 data set. J. Climate, 19, 446-469,
639 doi:10.1175/jcli3637.1.

640 Reverdin, G.: North Atlantic Subpolar Gyre Surface Variability (1895-2009). J. Climate, 23, 4571-4584,
641 doi: 10.1175/2010JCLI3493.1, 2010.

642 Saenko, O.A., Fyfe, J.C., and England, M.H.: On the response of the oceanic wind-driven circulation to
643 atmospheric CO_2 increase. Clim. Dynam., 25, 415-426, doi:10.1007/s00382-005-0032-5, 2005.

644 Schauer, U., Beszynnka-Möller, A., Walczowski, W., Fahrbach, E., Piechura, J., and Hansen, E.
645 Variations of measured heat flow through Fram Strait between 1997 and 2006, in: Arctic-subarctic
646 ocean fluxes, edited by Dickson, R.R., Meincke, J. and Rhines, P., Springer, Dordrecht, 65-85, 2008.

647 Schmidt, G.A., Jungclaus, J.H., Ammann, C.M., Bard, E., Braconnot, P., Crowley, T.J., Delaygue, G.,
648 Joos, F., Krivova, N.A., Muscheler, R., Otto-Bliesner, B.L., Pongratz, J., Shindell, D.T., Solanki, S.K.,
649 Steinhilber, F., Vieira, L.E.A.: Climate forcing reconstructions for use in PMIP simulations of the
650 last millennium (v.1.0), Geosci. Model Dev., 4, 33-45, doi:10.5194/gmd-4-33-2011 ,2011.

651 Serreze, M.C., Barnett, A.P., Slater, A.G., Steele, M., Zhang, J., and Trenberth, K. E.: The large-scale
652 energy budget of the Arctic. J. Geophys. Res., 112, D11122, doi:10.1029/2006JD008230, 2007.

653 Sedláček, J., and Mysak, L.A. A model study of the Little Ice Age and beyond: changes in ocean heat
654 content, hydrography and circulation since 1500. Clim. Dynam, 33, 461-475, doi: 10.1007/s00382-
655 008-0503-6, 2009.

656 Shaffrey, L., and Sutton, R.: Bjerknes compensation and the decadal variability of the energy
657 transports in a coupled climate model, J. Climate, 19, 1167-1448, doi:10.1175/JCLI3652.1, 2006.

658 Shi, F., Yang, B., Ljungqvist, F.C., and Yang, F.: Multi-proxy reconstruction of Arctic summer
659 temperatures over the past 1400 years, Clim. Res., 54, 113-128, doi:10.3354/cr01112, 2012.

660 Skagseth, Ø., Furevik, T., Ingvaldsen, R., Loeng, H., Mork, K.A., Orvik, K.A., and Ozhigin, V.: Volume
661 and heat transport to the Arctic Ocean via the Norwegian and Barents Sea, in: Arctic-subarctic
662 ocean fluxes, edited by Dickson, R.R., Meincke, J., and Rhines, P., Springer, Dordrecht, 45-64,
663 2008.

664 Smith, T.M., and Reynolds, R.W.: Improved extended reconstruction of SST (1854-1997). J. Climate,
665 17, 2466-2477, doi: 10.1175/1520-0442(2004)017<2466:IEROS>2.0.CO;2, 2004.

666 Spielhagen, R.F., Wagner, K., Sørensen, S.A., Zamelczyk, K., Kandiano, E., Budeus, G., Husum, K.,
667 Marchitto, T.M., and Hald, M.: Enhanced modern heat transfer to the Arctic by warm Atlantic
668 Water, Science 331 450-453, doi:10.1126/science.1197397, 2011.

669 Stevens, B., Giorgetta, M., Esch, M., Mauritsen, T., Crueger, T., Rast, S., Salzmann, M., Schmidt, H.,
670 Bader, J., Block, K., Brokopf, R., Fast, I., Kinne, S., Kornblueh, L., Lohmann, U., Pincus, R., Reichler,
671 T., and Roeckner, E.: Atmosphereric component of the MPI-M Earth system Model: Echam6, J.
672 Adv. Model Earth Syst., 5, 146-172, doi:10.1002/jame.20015, 2013.

673 Vieira, L.E.A., Solanki, S.K., Krivova, N.A., and Usoskin, I.: Evolution of the solar irradiance during the
674 Holcene, Astron. Astroph., 531, A6, doi:10.1051/0004-6361/201015843, 2011.

675 Wang, Y.-M., Lean, J.L., Sheeley Jr., N.R.: Modeling the Sun's magnetic field and irradiance since
676 1713, Astrophys. J., 625, 522-538, doi:10.1086/429689, 2005.

677 Werner, K., Spielhagen, R.F., Bauch, D., Hass, H.C., Kandiano, E., and Zamelcyk, K.: Atlantic water
678 advection to the eastern Fram Strait – multiproxy evidence for late Holocene variability,
679 Paleogeography, Paleoclimatology, Paleoecology, 308, 264-276, doi:10.1016/j.paleo.2011.05.030,
680 2011.

681 Zanchettin, D., Timmreck, C., Graf, H.-F. Rubino, A., Lorenz, S., Lohmann, K., Krüger, K., and
682 Jungclaus, J.H.: Bi-decadal variability excited in the coupled ocean-atmosphere system by strong
683 tropical volcanic eruptions, Clim. Dynam., 39, 419-444, doi:10.1007/s00382-011-1167-1, 2012.

684 Zanchettin, D., Timmreck, C., Bothe, O., Lorenz, S.J., Hegerl, G. Graf, H.-F., Luterbacher, J., and
685 Jungclaus, J.H.: Background conditions influence the decadal climate response to strong volcanic
686 eruptions. *J. Geophys. Res. Atmos.*, 118, doi:10.1002/jgrd50229, 2013.

687 Zhang, R., Delworth, T.L., Sutton, R., Hodson, D.L.R., Dixon, K.W., Held, I.M., Kushnir, Y., Marshall, J.,
688 Ming, Y., Msadek, R., Robson, J., Rosati, A.J., Ting, M.F., and Vecci, G.: Have aerosols caused the
689 observed Atlantic multidecadal variability? J. Atm. Sci., 70, 1135-1144, doi:10.1175/JAS-D-12-
690 0331.11, 2013.

691

692 **Figures**

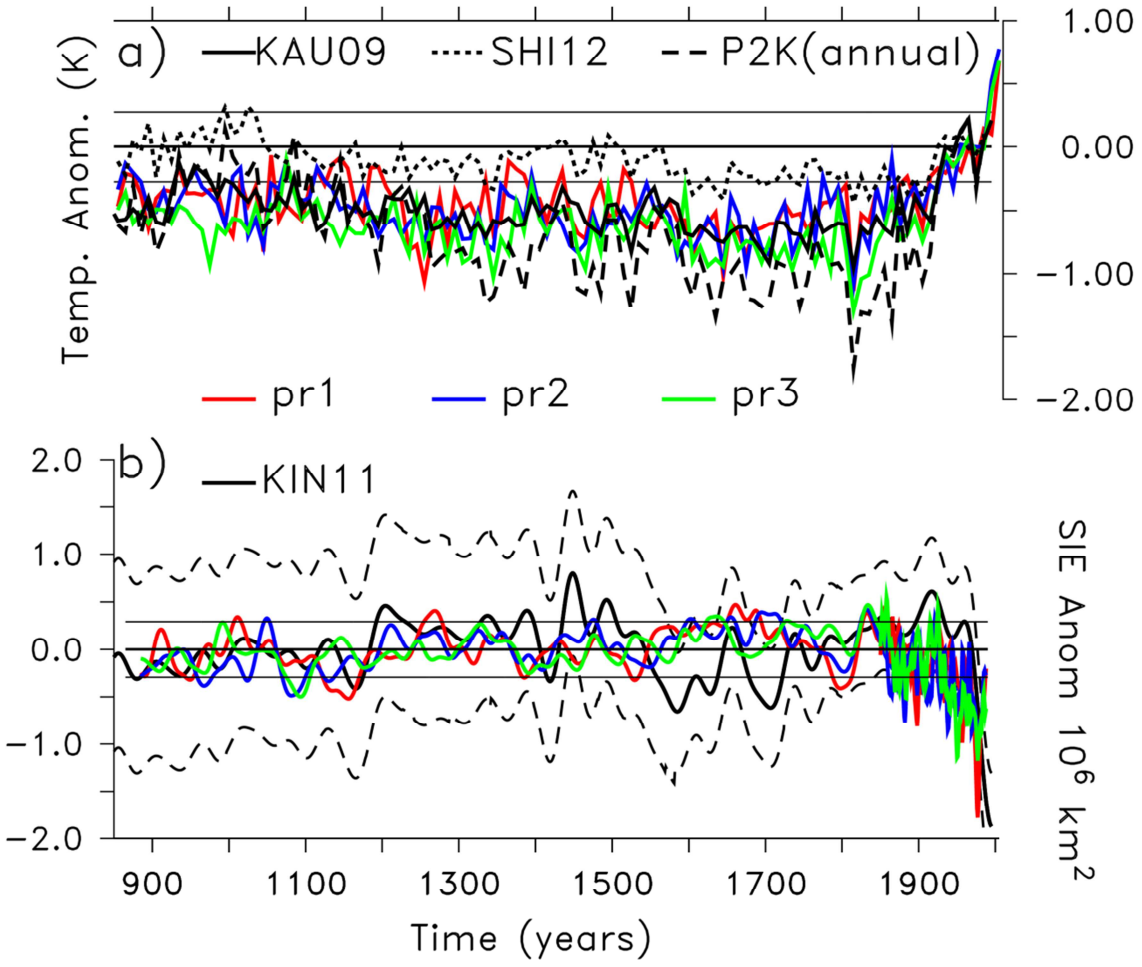

693

694

695 **Figure 1:** Simulated time series (colored lines for experiments pr1, pr2, pr3) of high northern latitude
696 climate variables in comparison with reconstructions (black lines): **a)** 10-year averages of Arctic
697 summer (JJA) surface air temperatures as anomalies w.r.t. the 1960-1990 mean. Summer
698 temperature reconstructions are from: (solid black) Kaufman et al. (2009), and (dotted black) Shi et
699 al. (2012). The PAGES2K reconstruction representing annual temperatures is also shown (dashed
700 black). **b)** late-summer (August) sea-ice extent (in 10^6 km^2) as anomalies w.r.t. the pre-industrial
701 mean in comparison with the reconstruction by Kinnard et al. (2011): The thick black line denotes the
702 40-year smoothed reconstruction, the dashed black lines their 95% confidence interval; for the
703 simulations, a 41-yr running mean was applied for pre-industrial millennium and a 5-yr running mean
704 for 1850-2005 to better display 20th century variability. Thin horizontal lines bracketing the zero line
705 in **a)** and **b)** indicate the respective 2σ-ranges derived from the 1000yr-long PiCtrl experiment.

706

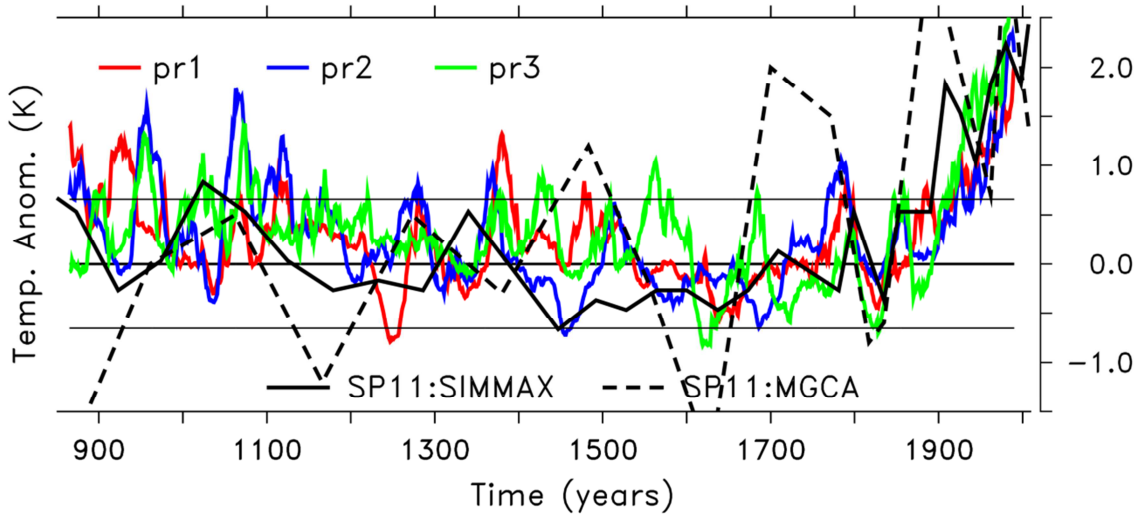

707

708 **Figure 2:** Simulated time series (colored lines for experiments pr1, pr2, pr3) of Atlantic Water
709 temperature anomalies w.r.t. the pre-industrial mean in Fram Strait (78°N, 50m depth) in comparison
710 with the reconstruction by Spielhagen et al. (2011) obtained by the (solid black) SIMMAX, and
711 (dashed black) Mg/Ca methods, respectively. The thin horizontal lines bracketing the zero line
712 indicate the respective 2σ-ranges derived from the 1000yr-long PiCtrl experiment.

713

714

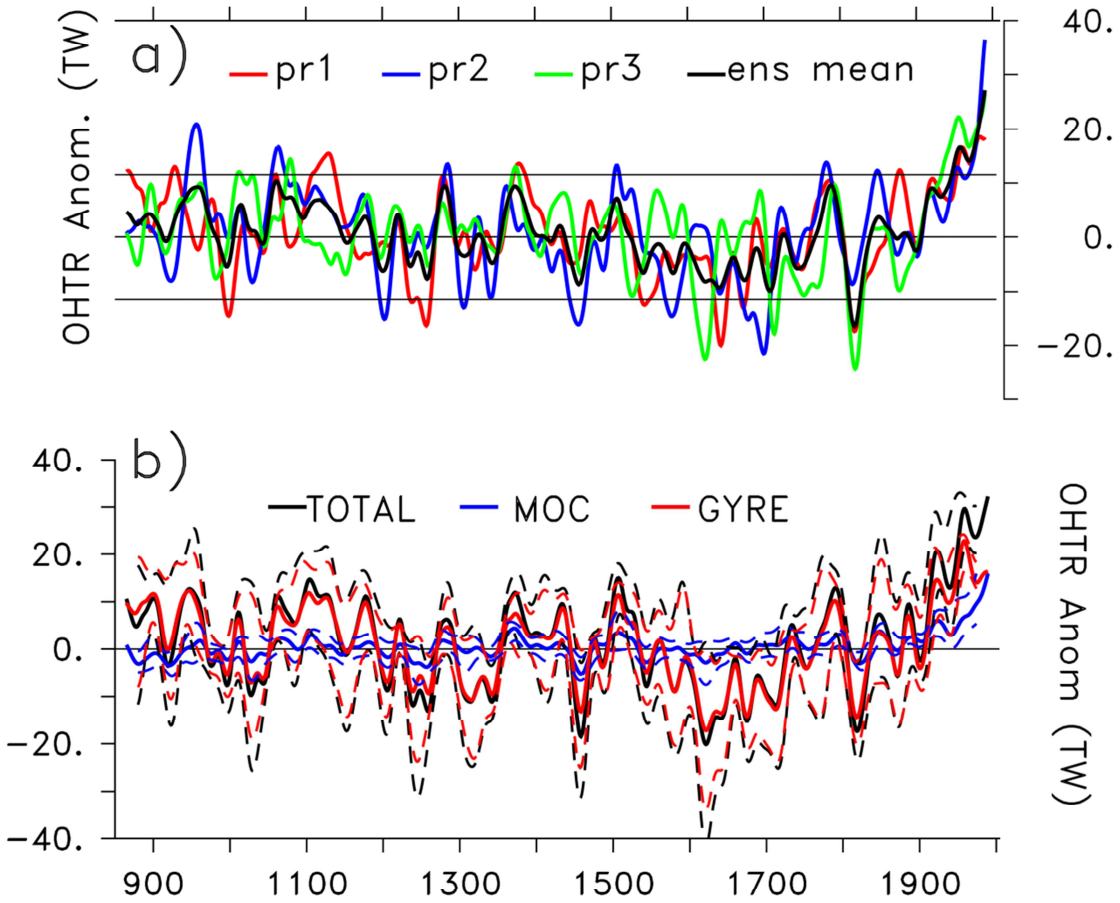

Figure 3: a) Simulated ocean heat transport (OHTR) to the Arctic (combined OHTR through Fram Strait and Barents Sea Opening) as anomalies w.r.t. the pre-industrial mean; colored lines indicate individual simulations pr1, pr2 and pr3, and the solid black line is the ensemble mean, thin horizontal lines bracketing the zero line indicate the respective 2σ-ranges derived from the 1000yr-long PiCtrl experiment. **b)** Total OHTR (black lines, TOHTR) averaged over 60-65°N, subdivided into gyre-related OHTR (red, GOHTR), and overturning-circulation-related OHTR (blue, MOHTR). Thick lines represent the ensemble means and the dashed lines the respective ensemble ranges. All time-series were smoothed by a 31-yr running mean. Units are TW (1 TW = 10^{12} Watt).

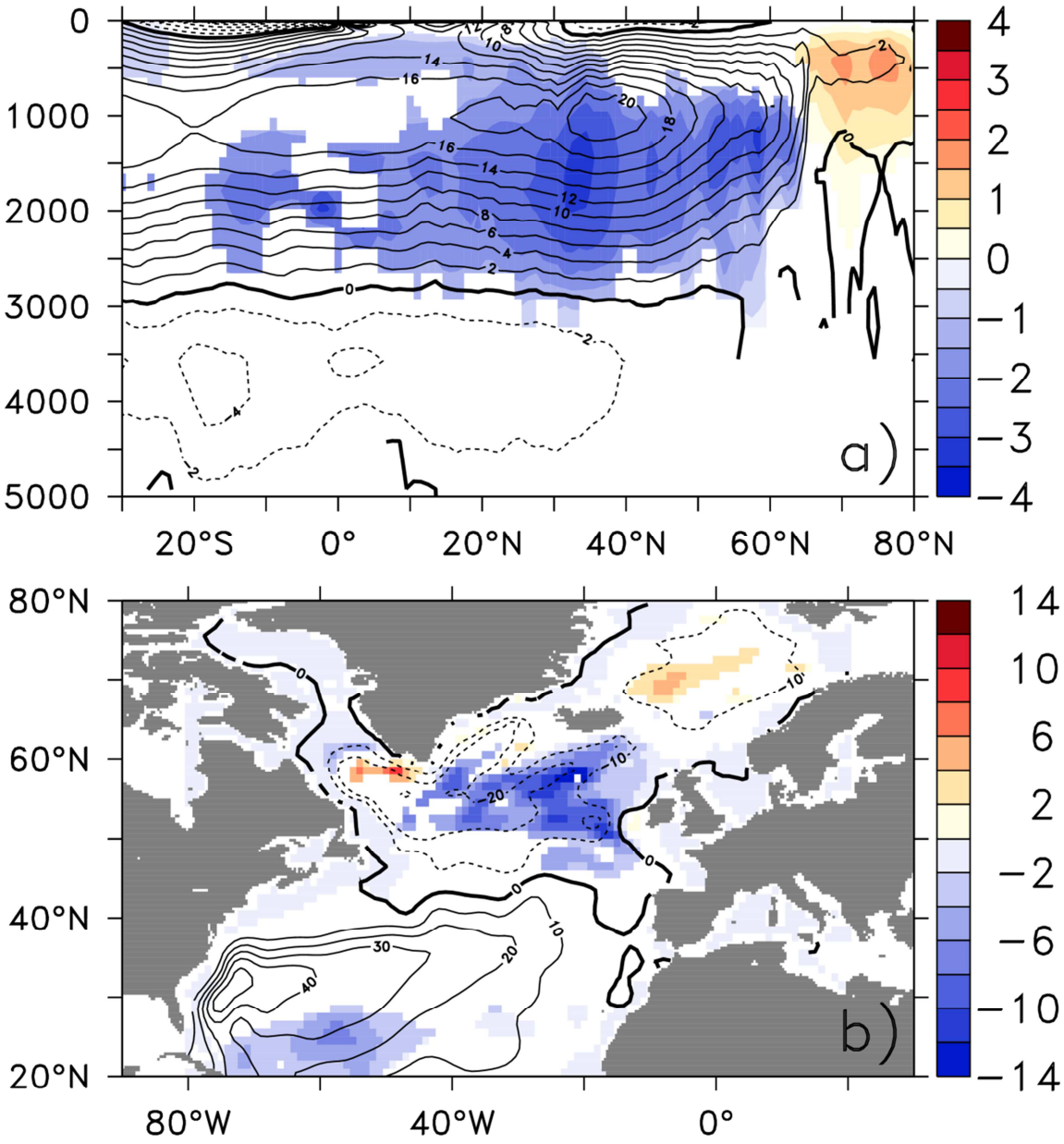

728

729

730 **Figure 4:** Simulated 20th century linear trends (1905-2005) in the pr2 simulation (color shading) of a)
731 meridional overturning circulation, and b) barotropic stream function in the North Atlantic. Units are
732 Sverdrups per 100 yrs (1 Sv = $10^6 m^3 s^{-1}$). Contour lines (contour intervals 2 SV for overturning and 10
733 Sv for barotropic stream function) describe the pre-industrial mean state. In both panels, only
734 anomalies are shown that exceed the 5-95 percentile range of centennial trends derived from the
735 PiCtrl simulations.
736

737

738

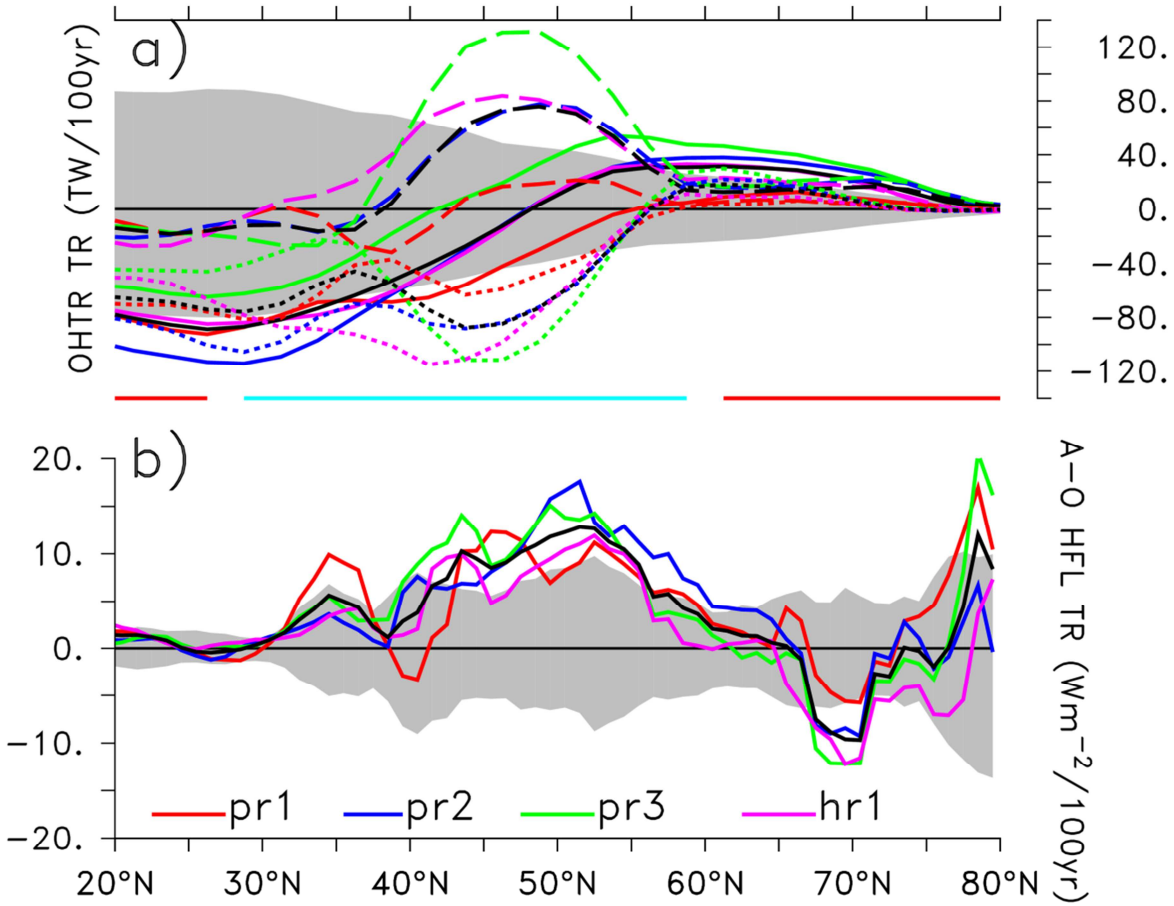

Figure 5: Simulated 20th century linear trends (1905-2005) as zonal averages over the Atlantic basin (experiments pr1, pr2, pr3, and hr1 as indicated by colored lines, black lines indicate ensemble means): **(a)** (solid lines) TOHTR, (dashed lines) GOHTR, and (dotted lines) MOHTR. Light-blue and red horizontal lines at the bottom of the plot indicate regions, where the ensemble-mean TOHTR divergence is positive (cooling by lateral advection: light-blue) or negative (warming by lateral advection: red). **(b)** atmosphere-ocean heat fluxes. Positive values indicate increased heat transfer from the atmosphere to the ocean or cooling of the atmosphere by the ocean. Colored lines are individual simulations and the black line is the ensemble mean. In **(a)** and **(b)**, the grey-shaded regions indicate the 5-95 percentile ranges of centennial trends in the unperturbed PiCtrl experiment.

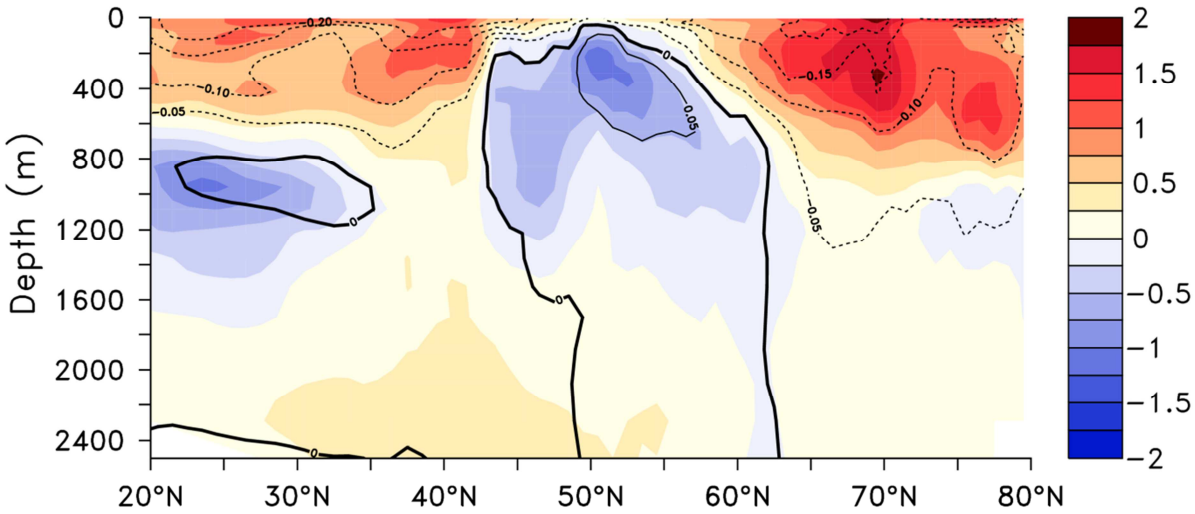

Figure 6: Simulated 20th century linear trends (1905-2005) as zonal averages over the Atlantic basin for potential temperature (color shading) and density (contours, contour interval 0.05 kgm^{-3}) trends from the pr2 experiment.

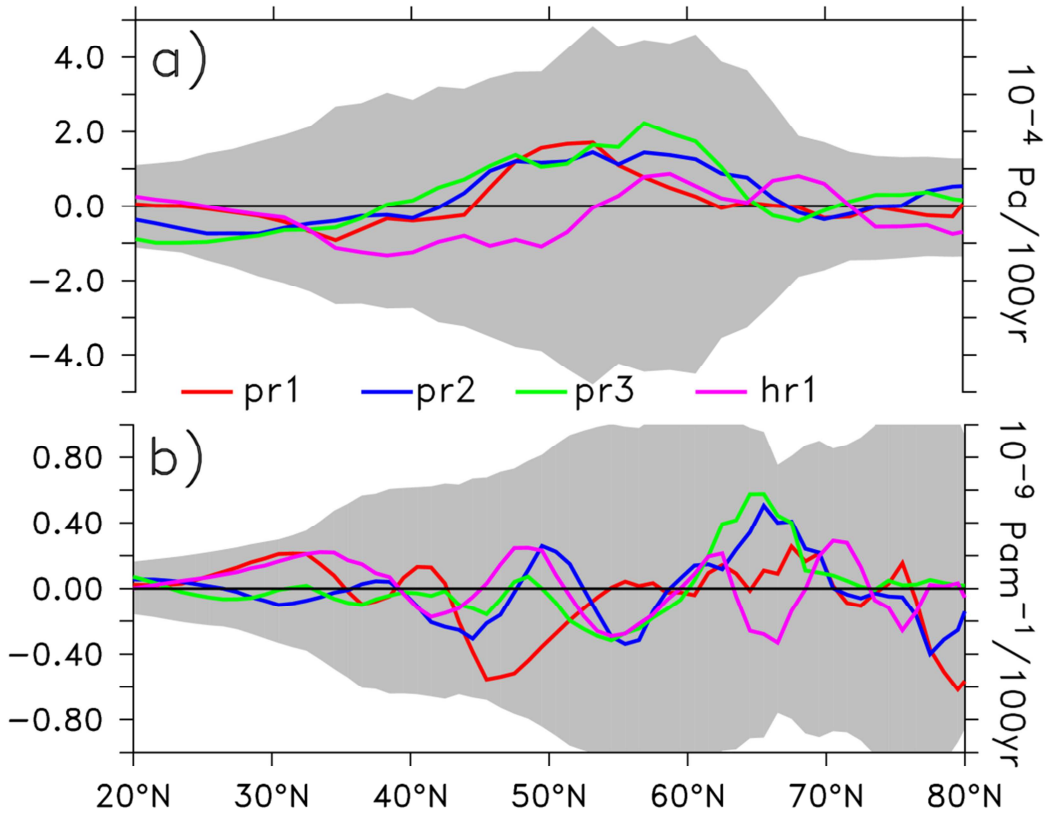

Figure 7: Simulated (experiments pr1, pr2, pr3, and hr1) 20th century linear trends (1905-2005) as zonal averages over the Atlantic basin of **(a)** zonal wind stress (units 10^{-2} Pa/100 yrs)and **(b)** wind stress curl (in 10^{-9} Pa m^{-1}/100yrs). Colored lines denote the experiments pr1, pr2, pr3, and hr1 and the grey-shaded regions bracketing the zero line show the 5-95 percentile range of centennial trends in the unperturbed PiCtrl experiment.

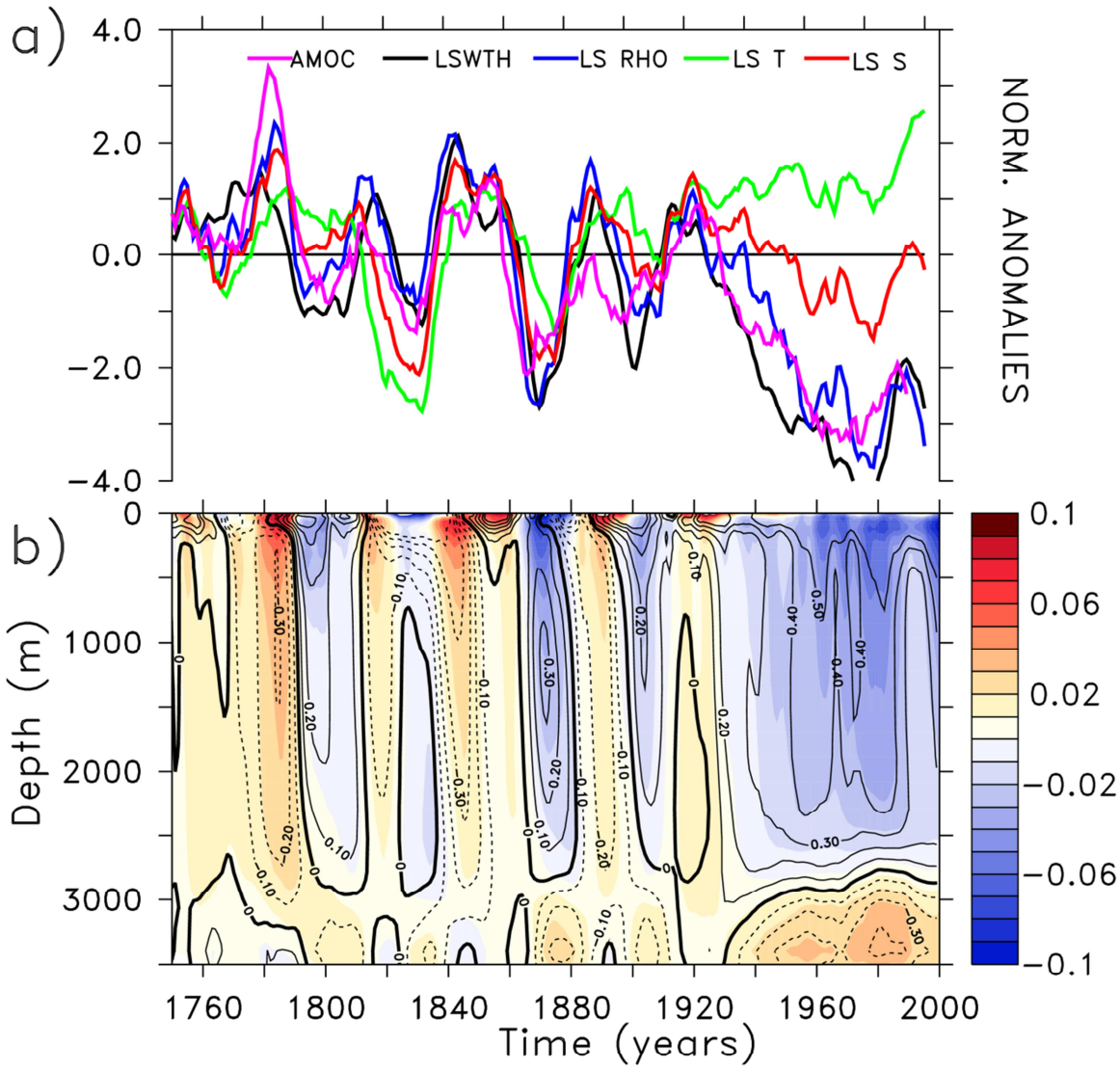

779

780 **Figure 8: (a)** Evolution of the Labrador Sea Water thickness (LSWTH, defined as the depth difference
781 between the isopycnals σ_2=36.74 and σ_2=36.82, averaged over 60W-45W, 50N-60N), AMOC stream
782 function at 30N and 1500m depth (displayed here with a 10-year time lag), and surface water mass
783 properties in the region, where convection takes place in the Labrador Sea: Density (LS RHO),
784 temperature (LS T), and salinity (LS S). All time-series are smoothed using an 11-yr running mean and
785 are shown as normalized anomalies w.r.t. the pre-industrial means. **(b)** Evolution of potential density
786 (color shading) and potential temperature (contours, contour intervals 0.05 K) as function of depth
787 and time for the Labrador Sea in the pr2 simulation. An 11-yr running mean was applied to the data.
788

789

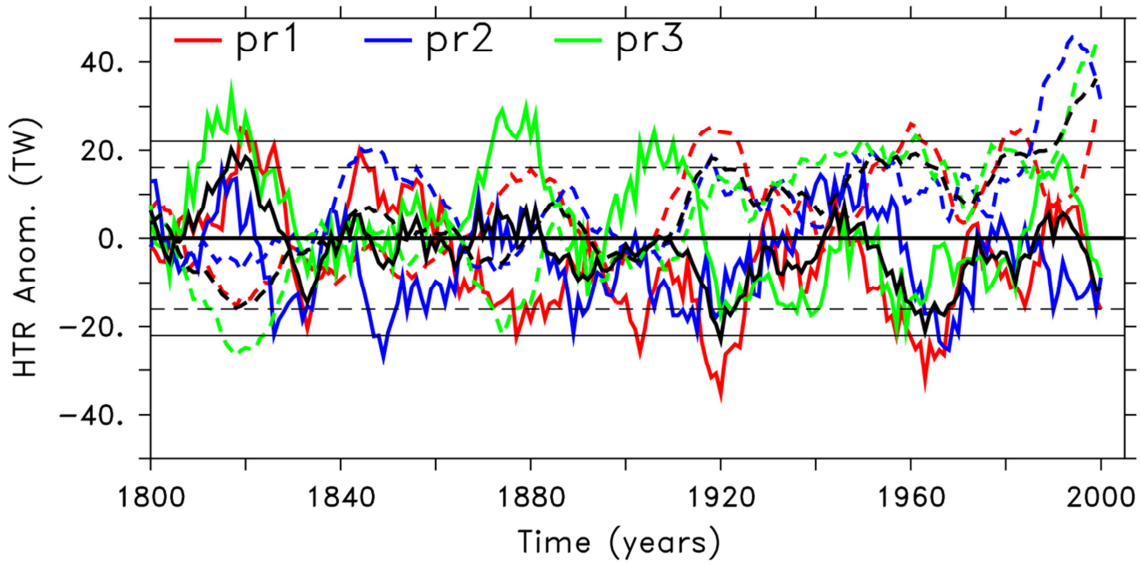

790

791 **Figure 9:** Time series of simulated (solid lines) atmospheric heat transports (AHTR) and (dashed lines)
792 TOHTR at 70°N as anomalies w.r.t. the pre-industrial mean (colored lines for experiments pr1, pr2,
793 pr3; time series shown as black dashed and solid lines denote the respective ensemble means).
794 The horizontal black lines bracketing the zero lines are the respective 2-σ ranges derived from the
795 PiCtrl experiment. An 11-yr running mean was applied to all data sets.

796